JACS
JOURNAL OF THE AMERICAN CHEMICAL SOCIETY
pubs.acs.org/JACS
Article

Common Defects Accelerate Charge Separation and Reduce Recombination in CNT/Molecule Composites: Atomistic Quantum Dynamics

Ritabrata Sarkar, Moumita Kar, Md Habib, Guoqing Zhou, Thomas Frauenheim, Pranab Sarkar,* Sougata Pal,* and Oleg V. Prezhdo*

Cite This: J. Am. Chem. Soc. 2021, 143, 6649−6656
Read Online

ABSTRACT: Carbon nanotubes (CNTs) are appealing candidates for solar and optoelectronic applications. Traditionally used as electron sinks, CNTs can also perform as electron donors, as exemplified by coupling with perylenediimide (PDI). To achieve high efficiencies, electron transfer (ET) should be fast, while subsequent charge recombination should be slow. Typically, defects are considered detrimental to material performance because they accelerate charge and energy losses. We demonstrate that, surprisingly, common CNT defects improve rather than deteriorate the performance. CNTs and other low dimensional materials accommodate moderate defects without creating deep traps. At the same time, charge redistribution caused by CNT defects creates an additional electrostatic potential that increases the CNT work function and lowers CNT energy levels relative to those of the acceptor species. Hence, the energy gap for the ET is decreased, while the gap for the charge recombination is increased. The effect is particularly important because charge acceptors tend to bind near defects due to enhanced chemical interactions. The time-domain simulation of the excited-state dynamics provides an atomistic picture of the observed phenomenon and characterizes in detail the electronic states, vibrational motions, inelastic and elastic electron−phonon interactions, and time scales of the charge separation and recombination processes. The findings should apply generally to low-dimensional materials, because they dissipate defect strain better than bulk semiconductors. Our calculations reveal that CNT performance is robust to common defects and that moderate defects are essential rather than detrimental for CNT application in energy, electronics, and related fields.

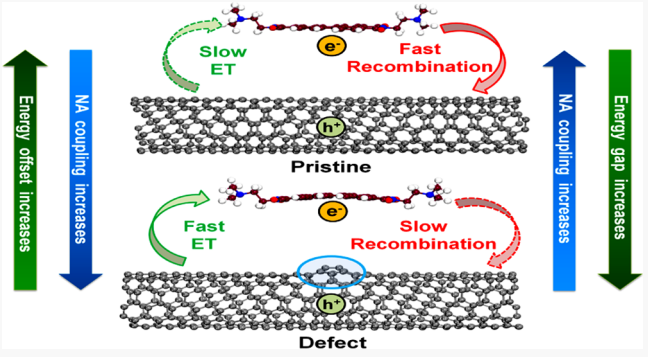

INTRODUCTION

Gradual depletion of fossil fuels leads to a significant energy crisis worldwide. In this context, the utilization of solar energy to generate fuels or electricity has attracted much attention for the management of future energy generation. A solar or photovoltaic cell is a device that converts the energy of sunlight into electricity.[1−6] It is important that solar cells satisfy the following three key attributes. First, absorption of light should lead to the generation of electron−hole (e−h) pairs.[7] Second, a photoinduced charge separation should occur at the interface between electron-donor and electron-acceptor materials.[8−12] Last, the separated charge carriers should be extracted to an external circuit.[13] Because charge transfer occurs downhill in energy, every charge-transfer step diminishes the achievable voltage. The e−h recombination leads to charge losses and reduces the current. Efficient solar cell performance requires that the charge separation and extraction are significantly faster than the recombination.

In the past decades, major attention has been paid to the fabrication of new, simple, and cost-effective photosensitizers for the utilization of solar energy into environment friendly electricity.[14−16] In this regard, metal-free carbon-based materials are promising for both light-absorption and charge transport.[17,18] Carbon nanotubes (CNT) have become a popular choice[19,20] among various carbon allotropes and derivatives. CNTs have demonstrated utility in many areas, including hydrogen storage technology,[21,22] field emission devices,[23,24] sensors,[25,26] nanoelectronic devices,[24,27,28] and solar cell devices.[20,29−32] In particular, small diameters and large aspect ratios of CNTs render them ideal one-dimensional quantum wires, a great asset for solar cells.[33−35] Depending on the energetic alignment of the highest occupied molecular

Received: March 1, 2021
Published: April 24, 2021

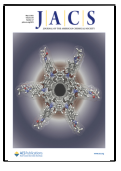

orbital (HOMO) and lowest unoccupied molecular orbital (LUMO) levels of the photosensitizing partners, CNTs can serve as either electron acceptors or electron donors.

Perylene derivatives represent a novel class of compounds having high photo and chemical stability.[36−38] In this context, perylenediimide (PDI) is a widely utilized molecular building block, because it shows exceptional optoelectronic properties and strong absorption in the visible region of the solar spectrum.[39] The extended aromatic system with a fused five-ring π-system makes perylenes suitable for $\pi-\pi$ stacking in particular with the CNT π-backbone.[40,41] It is well recognized that when PDIs are adsorbed on the CNT surface through $\pi-\pi$ stacking, the resulting hybrids exhibit many attractive optoelectronic properties.[42,43] Supramolecular construction of donor−acceptor conjugates has established itself as a superior approach, because of its relative simplicity and the possibility to interchange the donor and acceptor entities with relative ease.[44−46] Furthermore, this approach is nondestructive, as it preserves the intrinsic structure and electronic features of CNTs at the interface.[47,48] In these hybrids, CNTs function as electron donors, while PDIs serve as electron acceptors, promoting charge separation by electron transfer (ET) from CNTs to PDIs. Although the transfer of electrons from photosensitizers into semiconducting CNTs acting as electron acceptors is well established, the use of CNTs as electron donors is still scarce. The CNT/PDI composites constitute one of the few examples.

Recently, Tsarfati et al. investigated a composite, in which a PDI is noncovalently immobilized onto a CNT.[41] The charge transfer from CNT to PDI was reported to take 2−4 ps, while the charge relaxation to the ground state required a time period of below 50 ps. Excited-state photoinduced dynamics at heterojunctions between (6,5) CNTs and two PDI-based electron acceptors was investigated by Kang et al.[49] They demonstrated that photoinduced charge transfer produces long-lived charge-separated states. The charges recombined across the interface on time scales ranging from several picoseconds to microseconds. Donor−acceptor supramolecular hybrids based on CNTs and PDIs were studied by Guldi and co-workers.[50] The charge transfer from the donor CNT to acceptor PDIs occurred within 10 ps. The excited charges recombined within 200 ps. The photoexcited charge separation in CNT/perylene composites was investigated by Ehli et al., who demonstrated long-lived excited states after intersystem crossing, forming radical ion pairs at the interface.[51] Hedström et al. showed the spin-dependent e−h recombination between $Re^{I}(CO)_3(py)(bpy\text{-}Ph)$ and PDI. Spin-allowed e−h recombination is much faster (∼50 ps) than the spin-forbidden one (∼65 ns).[52] The experimental time scales for the charge separation and recombination differ significantly because of the diversity in composite geometries, the nature of the interactions, and the nonadiabatic (NA) couplings between the donor and acceptor states.

The presence of defects in CNTs can significantly alter their properties.[53,54] In the past, emphasis has been placed on the role of defects in accelerating charge carrier losses.[55,56] In comparison, the influence of defects on the photoinduced excited-state charge separation dynamics in CNT-based composites is nearly unexplored. However, the presence of defects in CNTs can play significant roles in controlling the charge-transfer dynamics when CNTs are coupled to suitable acceptors.

Herein, we investigate the ET and e−h recombination dynamics of CNT/PDI heterojunctions with and without defects. Employing the recently developed methodology combining real-time self-consistent-charge density functional tight-binding (SCC-DFTB) with NA molecular dynamics (MD),[57−59] we demonstrate that common CNT defects, including the 7557 and Stone−Wales (SW) defects, have a strong positive influence on both processes. This fact is surprising, because defects are commonly regarded as charge recombination centers, and significant efforts are dedicated to defect passivation and elimination. The conclusions drawn from the reported simulations apply to CNT-based composites in general and to other types of defects, as long as they create no deep trap states. The analysis shows that defects on CNT sidewalls perturb CNT electronic structure, leading to an accumulation of charge that creates an additional electrostatic potential and increases the CNT work function, lowering CNT energy levels relative to PDI. Because the molecular electron acceptor level is designed to reside inside the CNT band gap, the energy gap for the ET is decreased, while the energy gap for the e−h recombination is increased. As a result, the ET is accelerated, and the e−h is slowed, increasing charge separation, decreasing charge recombination, and improving the material's performance. The ET becomes 5- and 2-fold faster in the presence of the 7557 and SW defects, while the e−h recombination is slowed by 2 and 4 times, respectively, as compared to the pristine composite. The accelerated ET is rationalized by a stronger NA coupling between the donor and acceptor states in defect containing composites and activation of additional vibrational modes. The lowering of the e−h recombination rate is primarily due to a weaker NA coupling, increased energy gap, and decreased participation of low frequency vibrations. Both rapid charge separation and slow recombination are essential to achieve high photon-to-electron conversion efficiencies in solar cell devices. The findings can apply to other types of donor−acceptor hybrids based on low dimensional materials, which, in contrast to traditional bulk semiconductors, are capable of accommodating defects without creating deep mid gap charge trap states.

RESULTS AND DISCUSSION

The present work focuses on the photoinduced ET and e−h recombination dynamics at a CNT/PDI hybrid. Particular attention has been paid to the role of CNT defects (Figure 1a) in the excited-state dynamics. Two common defects, the 7557 and the SW, are introduced into the sidewall of the (6,5) CNT in the CNT/PDI hybrid. A photon absorption by the CNT results in multicomponent excited-state dynamics at the interface, as shown in Figure 1b. ET proceeds from the conduction band (CB) of the CNT to the PDI LUMO, generating an e−h pair in the CNT/PDI composite. In the presence of CNT defects, the charges can get trapped and lose mobility, if the trap states are energetically deep inside the CNT band gap. Mobile charges are extracted by the corresponding transport layers in a solar cell, while trapped charges eventually recombine by nonradiative relaxation to the ground electronic state. Efficient solar cell performance requires that the rate of charge separation is much faster than that of e−h recombination.

PDI is embedded onto the CNT surface by weak $\pi-\pi$ stacking. Introduction of the 7557 defect results in swelling of the π-surface, while the SW defect creates a dip in the CNT sidewall. Hence, to achieve an effective $\pi-\pi$ interaction, PDI

https://doi.org/10.1021/jacs.1c02325
J. Am. Chem. Soc. 2021, 143, 6649−6656

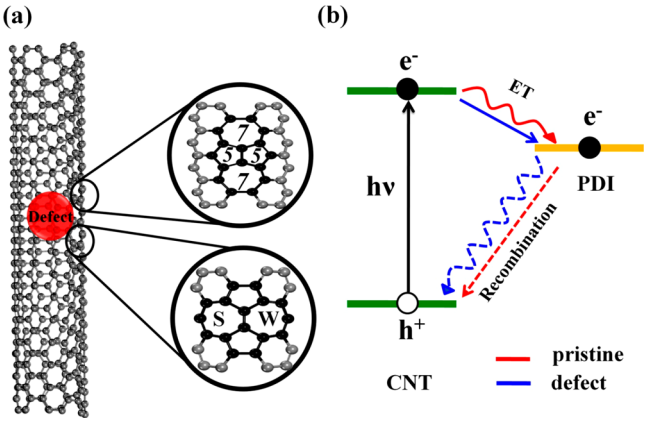

Figure 1. (a) The 7557 and SW defects in the (6,5) CNT. The 7557 defect arises from insertion of a C_2 dimer into the six-member benzene ring and creates a bulge on the CNT surface. It creates two pentagon and two heptagon rings. The SW defect is a C_2 rotation within the ideal hexagonal lattice of the CNT. It also creates two pentagon and two heptagon rings, but without the bulge. (b) Schematic of the energy levels involved in the photoinduced charge dynamics at the CNT/PDI heterointerface. An e−h pair is generated in the CNT upon photon absorption. The excited electron then is transferred from the CNT CB to the PDI LUMO. Following the charge separation, the e−h pair may undergo recombination across the interface. The 7557 and SW defects do not create deep mid gap trap states, but they change the CB and VB alignment relative to the PDI LUMO (Figures 2 and 3).

bends around the 7557 defect site, while PDI moves away from the SW defect site, as shown in Figure S1. The calculated energies of interaction between the CNT and PDI show that all CNT/PDI hybrids are thermodynamically stable (Table S2). Because side wall defects disrupt π-electron conjugation of the CNT, and since the CNT−PDI interaction proceeds through $\pi-\pi$ stacking, the defective hybrids are slightly destabilized relative to the pristine system. The composites remain stable at 300 K, with their π-stacking intact (Figure S2).

The concentration of sidewall defects in CNTs can be quantified by $(N_{defect}/N_{atom}) \times 100$, where N_{defect} and N_{atom} denote the number of defects and total number of atoms in the pristine CNT, respectively. The systems under investigation contain one defect per 364 atom unit cell of the (6,5) CNT. Thus, the defect concentration is 0.274% for both defects. Defect concentration is significantly lower in experiments. For instance, using the intensity ratio of the D and G bands in the Raman spectra, Vinten et al. showed that the defect density for the pentagon−heptagon defect pair is 2.3×10^{-6} defects/carbon, or equivalently 1 defect per 4.4×10^5 carbon atoms.[60] Calculations provide similar estimates.[61] It is impossible to achieve comparable defect concentration in an atomistic simulation, because it would require thousands of electronic structure calculations on systems composed of one-half a million atoms. Our study describes a situation in which the molecular species is adsorbed close to a defect site. We demonstrate that, in such a case, the common defects are favorable rather than detrimental for the charge separation and recombination processes in solar energy applications. This is an important finding, because it is assumed typically that defects provide the main mechanism of charge and energy losses. We also characterize the situation in which the molecular species are adsorbed on defect-free parts of CNTs.

The key factors governing the excited-state dynamics include the relative energies of the charge donor and acceptor states and the localization of the corresponding wave functions. The offset between the CNT band edges and the PDI HOMO and LUMO represents a type-II heterostructure, which is preserved in the presence of the two defects (Figure 2). MD simulations demonstrate that the type-II alignment is maintained at 300 K. The driving force for the ET is measured by the energy gap between the CNT CB and the PDI LUMO. The driving force should overcome the exciton binding energy (EBE), which is the measure of Coulomb attraction between e and h in the CNT. Experimental EBE for the (6,5) CNT is in the range of 0.20−0.40 eV depending on the dielectric environment of the medium.[62,63] At 300 K, the canonically averaged band offset for the ET is 0.269 eV in the pristine system and is slightly decreased for the CNTs with the defects (Table 1). It is important to note that the 7557 and SW defects perturb the CNT electronic structure only moderately. Neither defect creates a mid gap trap state, nor do the defects change significantly the value of the band gap.

The charge densities of the key orbitals, including PDI LUMO, CNT valence band maximum (VBM), conduction band minimum (CBM), and CBM+1, involved in the charge-transfer dynamics of the CNT/PDI composites are shown in Figure S3. The charge densities of the VBM, CBM, and CBM +1 states of pristine CNT are fully delocalized. On the other hand, the defects moderately localize the CBM and VBM charge densities, with the largest localization observed for the VBM in the composite with the 7557 defect. The CBM+1

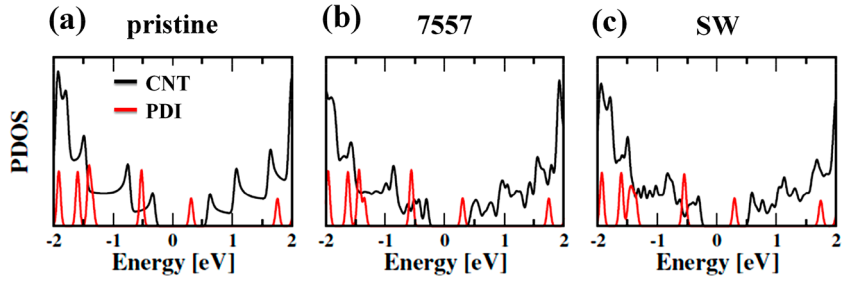

Figure 2. Projected density of states (PDOS) of the interacting CNT and PDI systems in (a) the pristine CNT/PDI composite, and the composite with (b) 7557 and (c) SW defects. All the composites show type-II band alignment, with the HOMO of the combined system corresponding to the CNT VBM and the LUMO localized on the PDI. Of note, the CNT DOS is larger than the PDI DOS. The nature of the CNT van Hove singularities and the PDI discrete energy levels is preserved in the combined system. The van Hove singularities are perturbed only slightly by the defect. The chemical environment and hence the electronic features of the CNT are unaffected by the PDI, implying that the interaction between the PDI and the CNT remains noncovalent in nature.

https://doi.org/10.1021/jacs.1c02325
J. Am. Chem. Soc. 2021, 143, 6649−6656

Table 1. Simulated Averaged Band Offset/Gap, Root-Mean-Square NA Electron−Phonon Coupling, Decoherence, and Relaxation Times for ET and e−h Recombination in the CNT/PDI Hybrids

process	systems	band offset/gap (eV)	NA coupling (meV)	decoherence (fs)	time scale (ps)
ET	pristine	0.269	2.73	26.2	10
	7557	0.207	49.03	28.1	1.8
	SW	0.253	7.56	23.4	5.9
e−h recombination	pristine	0.483	1.83	6.2	137
	7557	0.520	1.49	4.7	231
	SW	0.555	0.83	7.6	548

charge density remains delocalized even in the defective CNTs. The LUMO is fully localized in PDI for all composites. The localization of the VBM of the CNTs with the defects near the PDI facilitates interaction of the CNT and PDI π-electron subsystems and favors rapid ET from the CNT to PDI. In comparison, delocalization of the CBM charge density over the defect-free CNT disfavors charge transfer to PDI in the pristine composite.

The CNT and PDI are noncovalently attached by van der Waals force of attraction, and a local electrostatic interaction is present between the CNT and PDI due to an asymmetric charge distribution. The Mulliken charge distribution analysis reveals that the Coulomb interaction is stronger in the systems containing defects than in the pristine composite, and the trend is 7557 > SW > pristine. The additional electrostatic potential increases the material's work function and shifts the energy levels of the defective composites down in energy[64] (Figure 3). The charge distribution of the pristine CNT is perturbed by the defects (Figure S4), the CNT electrostatic properties change more than those of PDI, and the CNT energy levels are shifted down relative to PDI's LUMO (Figure 3). The larger shift of the CBM energy as compared to the LUMO rationalizes the decrease of the band offset for the ET

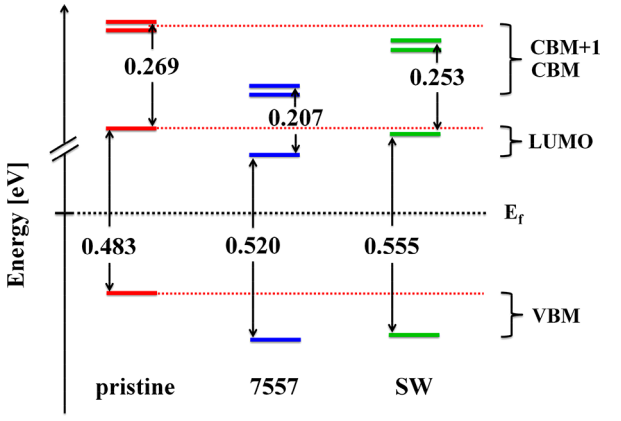

Figure 3. Schematic of the key energy states involved in the charge separation and recombination dynamics in the composite systems. The energy levels are shifted to lower energies in the presence of defects, due to stronger electrostatic interactions and increased work functions (Table S1). The downshift is larger for the CNT states because of the CNT defects. As a result, the energy gap for the charge separation decreases, favoring fast ET, while the energy gap for the charge recombination increases, favoring longer-lived charge-separated states.

in the defected composites (Table 1). This phenomenon favors efficient charge separation. At the same time, the larger shift of the VBM energy relative to the LUMO increases the energy gap for the e−h recombination, extending the lifetime of the charge-separated state.

The favorable change in the energy gaps to facilitate faster charge separation and slower charge recombination relies on the fact that the defects create only a moderate perturbation to the CNT properties. Defects creating deep mid gap trap states can accelerate charge separation, but they will also accelerate the recombination. The 7557 defect reduces the CBM−LUMO gap for the ET more than does the SW defect (Table 1), because generally it perturbs the CNT properties more significantly. At the same time, the SW defect increases the LUMO−VBM gap for the e−h recombination more than does the 7557 defect, because the 7557 defect perturbs the VBM to a larger extent than does the SW defect (Figure 3) and lifts its energy.

The shift of the CNT energy levels by the defects is corroborated with the work functions reported in Table S1. Calculated with DFT, the work functions follow the trend 7557 > SW > pristine. Thus, the additional electrostatic potential arising due to perturbation of the CNT electronic system by the defects is strongest in the 7557 system, and the electrostatic lowering of the CNT VBM and CBM levels relative to the PDI LUMO is more significant.

The photoinduced charge separation and recombination at the CNT/PDI interface occur by nonradiative transitions, and therefore these processes are strongly coupled to vibrational motions. Both elastic and inelastic electron−vibrational interactions play important roles. Elastic scattering randomizes phases of the electronic wave functions that in turn leads to loss of quantum coherence, whereas inelastic scattering is responsible for loss of electronic energy as heat during the charge-transfer processes. Thus, to gain a deeper insight into the dynamics, knowledge of charge−phonon interactions is crucial in this context.

For a particular system, not all the vibrational modes are available for coupling to the electronic subsystem during the photoinitiated excited-state dynamics. Fourier transforms (FTs) of the energy gaps between the donor and acceptor states, known as the influence spectra or spectral densities, characterize the phonon modes coupled to the electronic subsystem. Figure 4 presents the data for the ET process, while Figure 5 gives the influence spectra for the e−h recombination in the three composites. The high-frequency phonon mode at 1750 cm^{-1} is due to C−C stretching in the CNT, well-known as the G band.[65] The strong peak at 1550 cm^{-1} is due to the in-plane C=C stretching motion of the PDI aromatic core.[66] The less dominant peaks around 1600−1650 cm^{-1} are ascribed to the C=O phonon vibration of PDI.[67] Low frequencies under 500 cm^{-1} arise from radial breathing modes (RBM) of CNT[31,68] and substituent-assisted plane distortions of the PDI core.[69] The high-frequency phonon modes in the range of 1500−1800 cm^{-1} drive the ET process. Only these modes are seen in the signal for the pristine system (Figure 4a). Defects break the CNT symmetry and introduce and activate other modes, in particular in the lower frequency range (Figure 4b and c). The incorporation of an extra C_2 dimer and the C_2 rotation perturb the π-surface of the CNT, creating local vibrational modes in the RBM frequency range. Coupling of the wider range of vibrational modes increases the NA coupling and accelerates the ET process (Table 1). Both high

https://doi.org/10.1021/jacs.1c02325
J. Am. Chem. Soc. 2021, 143, 6649−6656

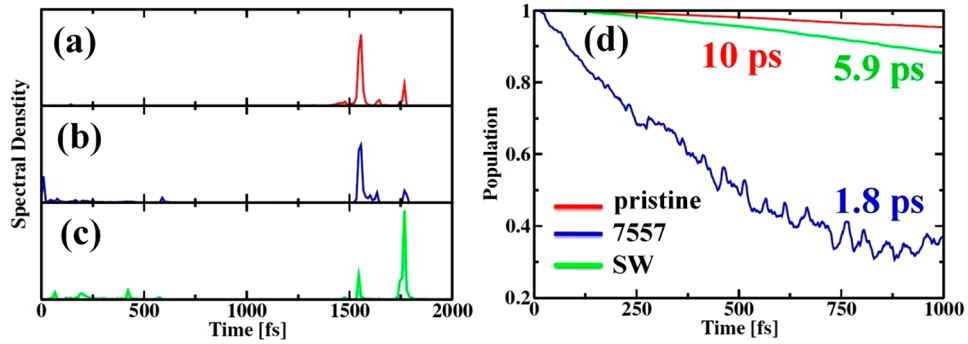

Figure 4. Fourier transforms (FTs) of the energy gaps between the donor and acceptor states involved in the photoinduced ET in the (a) pristine, (b) 7557, and (c) SW composites. The ET is driven by high frequency phonons that are capable of accommodating larger amounts of energy lost during the process. The defects activate additional modes in the lower frequency range. (d) The ET dynamics at the CNT/PDI interface. Shown are evolutions of populations of the photoexcited states. The 7557 and SW defects accelerate the ET by factors of 5 and 2, respectively.

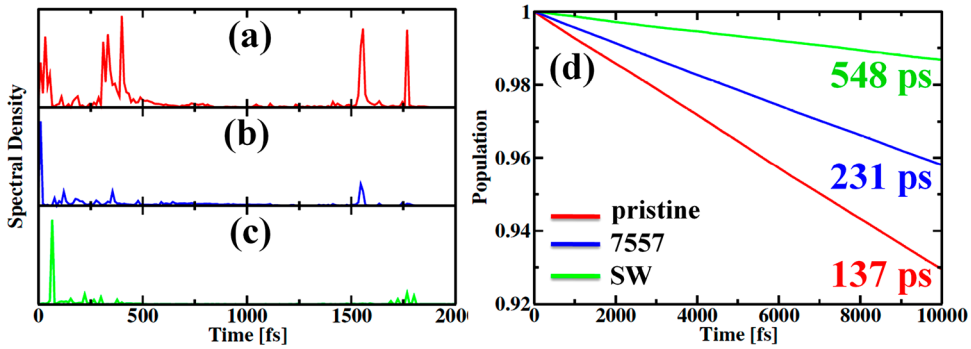

Figure 5. Fourier transforms (FTs) of the energy gaps between the donor and acceptor states involved in the e−h recombination dynamics in (a) pristine, (b) 7557, and (c) SW composites. A broad range of vibrations participate in the recombination process. While higher frequency modes can accommodate larger amounts of electronic energy and have higher velocities that enter the NA coupling, lower frequency modes have a stronger influence on the e and h wave functions and produce larger nuclear gradient matrix elements. The defect deactivates some of the higher frequency phonons and generally makes the electron−phonon coupling weaker (Table 1). (d) The e−h recombination for the systems under consideration. Shown are evolutions of populations of the charge-separated states. The 7557 and SW defects extend the lifetime of the charge-separated states by factors of 2 and 4, respectively.

and low frequency vibrations are involved in the e−h recombination process (Figure 5). While the ET process is too fast to allow significant contributions from the slow vibrational motions, the e−h recombination takes a much longer time. The slow out-of-plane motions that perturb the π-electron systems of the CNT and PDI and modulate their overlap play important roles during the recombination.

We compute the decoherence time as the pure-dephasing time of the optical response theory, by applying the second-order cumulant approximation.[70] The pure-dephasing functions are fitted with Gaussians $y = \exp(-0.5[t/\tau_{decoh}]^2)$ to obtain the decoherence times, τ_{decoh}, reported in Table 1. The decoherence times are longer for the ET than for the e−h recombination. The 7557 defect extends coherence for the ET process and shortens it for the recombination as compared to pristine CNT, but the SW defect shows the opposite trend. The duration of coherence present between pairs of states influences the carrier dynamics. However, other factors such as the NA coupling, energy offsets and gaps, and participating phonon modes have a stronger influence than does the coherence time, making the systems with defects perform better than the pristine system. Overall, the decoherence time scales for ET and e−h recombination for defects are comparable to those for the pristine structure. All these facts favor faster charge separation and slower recombination, because faster decoherence leads to slower dynamics, as exemplified by the quantum Zeno effect.[71]

The ET from the photoexcited CNT to PDI proceeds through a NA transition between the CBM and LUMO. The results of the NAMD simulations of the ET process are presented in Figure 4d. The decay curves are fitted by a linear combination of the Gaussian and exponential functions, $y = A \exp(-t/\tau_{exp}) + (1-A) \exp(t/\tau_{gau})^2$, and the reported time scales are the weighted averages of the two time constants, $\tau = A\tau_{exp} + (1 - A)\tau_{gau}$. Photoexcitation of the CNT in the pristine composite leads to ET to the PDI with a time constant of 10 ps. This agrees with the recent experiments reporting the charge-transfer time of below 50 ps in (6,5) CNT/PDI.[72] The defects accelerate the transfer by a factor of 2−5, with the 7557 defect having a stronger influence. The accelerated charge separation arises as a result of several factors. The CBM−LUMO energy gaps decrease because the CNT CBM shifts down in energy due to both increased work function (Table S1) and modest localization of the CBM around the defects. Both factors lower the CBM energy. The NA coupling for the CBM−LUMO transition increases in the composites containing the defects (Table 1). Lowering of the energy gap contributes to the increased NA coupling. Other factors include localization of the CBM near the defects that provide adsorption sites for the PDI molecules (Figures S3 and S4) and additional coupling of low frequency vibrations to the NA

https://doi.org/10.1021/jacs.1c02325
J. Am. Chem. Soc. 2021, 143, 6649−6656

transition (Figure 4). Cumulatively, all of these factors play positive roles, favoring efficient charge separation and leading to improved device performance.

The e−h recombination constitutes the primary source for the undesired energy and current losses, limiting device performance. Not only a rapid charge transfer between donor and acceptor is required to enhance the efficiency of a solar cell, but also slow and delayed e−h recombination is highly desired. The results of the NAMD simulation of the e−h recombination shown in Figure 5d have been fitted to the exponential function $y = \exp(-t/\tau)$ to obtain the recombination time constants summarized in Table 1. The 137 ps time obtained for the pristine composite provides a good match with the experimental result (630 ps).[72] The defects slow the recombination by a factor of 2−4, to 231 ps for 7557 and 548 ps for SW. The influence of defects on the carrier relaxation dynamics can be traced by the following factors. The defects increase the CNT work functions (Table S1), shifting the CNT energy levels down, and hence increase the gap between the PDI LUMO and the CNT VBM (Figure 3). The increased gap leads to slower relaxation, according to the exponential gap law.[73] The defects suppress participation of the low frequency modes in the e−h recombination dynamics. Parts b and c of Figure 5 show much weaker signals in the 250−500 cm^{-1} frequency range as compared to part a. The increased energy gap and decreased number of active vibrational modes lead to smaller NA coupling in the defective composites (Table 1). Thus, in addition to the faster ET, the 7557 and SW defects favor slower e−h recombination. Both phenomena assist in improving the performance of photovoltaic and electrooptic devices.

CONCLUSION

By combining the time-domain SCC-DFTB method with NAMD, we have investigated the ET and e−h recombination in the CNT/PDI nanohybrids. The simulation explored the role of CNT defects (7557 and SW) in the photoinduced excited-state dynamics. The time scales obtained for both the ET and the e−h recombination events nicely corroborate with the recent experimental observations. The simulated ET time scales for the pristine, 7557, and SW defect systems are 10, 1.8, and 5.9 ps, respectively. The charge redistribution induced by the defects enhances the local electrostatic interaction and increases the CNT work function. As a result, the defects lower the donor−acceptor energy gap for the photoinduced ET, and thereby the NA coupling becomes stronger, and the ET rate increases as compared to the pristine system. The accelerated ET is also favored by the involvement of a broader range of vibrational modes in the defect presence. On the other hand, the e−h pair recombines in the pristine system within 137 ps, while the 7557 defect extends the charge lifetime nearly by a factor of 2 to 231 ps. The SW defect slows the recombination even more, enhancing the carrier lifetime to 548 ps. Defects increase the energy gap for the e−h recombination, as compared to the pristine system, because the CNT VBM is shifted toward a lower energy relative to the PDI level. In addition, the defects deactivate low frequency vibrations involved in the recombination. By weakening the NA coupling, the defects suppress the nonradiative e−h recombination and promote longer-lived charge-separated states. Chemical interactions are enhanced by defects, and many molecules, polymers, and other acceptor species tend to bind near defect sites. The obtained conclusion that common CNT defects favor charge carrier separation and slow charge carrier recombination in CNT composites is very important for solar energy applications. By establishing the detailed atomistic mechanism of this phenomenon, the study suggests that the conclusion may apply to defects in other low dimensional materials that can accommodate defect-induced strain and avoid creating localized mid gap charge traps that are common in traditional bulk semiconductors.

ASSOCIATED CONTENT

Supporting Information

The Supporting Information is available free of charge at https://pubs.acs.org/doi/10.1021/jacs.1c02325.

Details of simulation methods, geometries at 0 and 300 K, charge density distribution, along with work function and Mulliken charge distributions of pristine and defect CNT/PDI composites (PDF)

AUTHOR INFORMATION

Corresponding Authors

Pranab Sarkar − *Department of Chemistry, Visva-Bharati University, Santiniketan 731235, India*; Email: pranab.sarkar@visva-bharati.ac.in

Sougata Pal − *Department of Chemistry, University of Gour Banga, Malda 732103, India*; orcid.org/0000-0002-1514-2728; Email: sougatapal_1979@yahoo.co.in

Oleg V. Prezhdo − *Department of Chemistry, University of Southern California, Los Angeles, California 90089, United States*; orcid.org/0000-0002-5140-7500; Email: prezhdo@usc.edu

Authors

Ritabrata Sarkar − *Department of Chemistry, University of Gour Banga, Malda 732103, India*

Moumita Kar − *Department of Chemistry, Visva-Bharati University, Santiniketan 731235, India*

Md Habib − *Department of Chemistry, University of Gour Banga, Malda 732103, India*

Guoqing Zhou − *Department of Physics and Astronomy, University of Southern California, Los Angeles, California 90089, United States*; orcid.org/0000-0002-4000-8467

Thomas Frauenheim − *Bremen Center for Computational Materials Science, University of Bremen, Bremen 28359, Germany; Shenzhen JL Computational Science and Applied Research Institute (CSAR), Shenzhen 518110, China; Beijing Computational Science Research Center (CSRC), Beijing 100193, China*

Complete contact information is available at: https://pubs.acs.org/10.1021/jacs.1c02325

Notes

The authors declare no competing financial interest.

ACKNOWLEDGMENTS

P.S. and S.P. acknowledge the financial support from DST Nano-Mission (SR/NM/NS-1005/2016(G)). S.P. acknowledges the financial support from CSIR (01(2956)/18/EMR-II), Government of India. R.S. and M.K. are grateful to CSIR for Senior Research Fellowships. O.V.P. acknowledges the financial support from the U.S. National Science Foundation, grant no. CHE-1900510.

REFERENCES

(1) O'regan, B.; Grätzel, M. A low-cost, high-efficiency solar cell based on dye-sensitized colloidal TiO 2 films. *Nature* **1991**, *353* (6346), 737−740.

(2) Ballesteros, B.; de la Torre, G.; Ehli, C.; Aminur Rahman, G.; Agulló-Rueda, F.; Guldi, D. M.; Torres, T. Single-wall carbon nanotubes bearing covalently linked phthalocyanines− photoinduced electron transfer. *J. Am. Chem. Soc.* **2007**, *129* (16), 5061−5068.

(3) Adegoke, O. O.; Jung, I. H.; Orr, M.; Yu, L.; Goodson, T., III Effect of acceptor strength on optical and electronic properties in conjugated polymers for solar applications. *J. Am. Chem. Soc.* **2015**, *137* (17), 5759−5769.

(4) Kim, S.; Márquez, J. A.; Unold, T.; Walsh, A. Upper limit to the photovoltaic efficiency of imperfect crystals from first principles. *Energy Environ. Sci.* **2020**, *13* (5), 1481−1491.

(5) Khenkin, M. V.; Katz, E. A.; Abate, A.; Bardizza, G.; Berry, J. J.; Brabec, C.; Brunetti, F.; Bulović, V.; Burlingame, Q.; Di Carlo, A.; Cheacharoen, R.; Cheng, Y.-B.; Colsmann, A.; Cros, S.; Domanski, K.; Dusza, M.; Fell, C. J.; Forrest, S. R.; Galagan, Y.; Di Girolamo, D.; Grätzel, M.; Hagfeldt, A.; von Hauff, E.; Hoppe, H.; Kettle, J.; Köbler, H.; Leite, M. S.; Liu, S. F.; Loo, Y.-L.; Luther, J. M.; Ma, C.-Q.; Madsen, M.; Manceau, M.; Matheron, M.; McGehee, M.; Meitzner, R.; Nazeeruddin, M. K.; Nogueira, A. F.; Odabası, Ç.; Osherov, A.; Park, N.-G.; Reese, M. O.; De Rossi, F.; Saliba, M.; Schubert, U. S.; Snaith, H. J.; Stranks, S. D.; Tress, W.; Troshin, P. A.; Turkovic, V.; Veenstra, S.; Visoly-Fisher, I.; Walsh, A.; Watson, T.; Xie, H.; Yıldırım, R.; Zakeeruddin, S. M.; Zhu, K.; Lira-Cantu, M. Consensus statement for stability assessment and reporting for perovskite photovoltaics based on ISOS procedures. *Nat. Energy* **2020**, *5* (1), 35−49.

(6) Huang, Y.-T.; Kavanagh, S. R.; Scanlon, D. O.; Walsh, A.; Hoye, R. L. Perovskite-inspired materials for photovoltaics and beyond—from design to devices. *Nanotechnology* **2021**, *32* (13), 132004.

(7) Freitag, M.; Teuscher, J.; Saygili, Y.; Zhang, X.; Giordano, F.; Liska, P.; Hua, J.; Zakeeruddin, S. M.; Moser, J.-E.; Grätzel, M. Dye-sensitized solar cells for efficient power generation under ambient lighting. *Nat. Photonics* **2017**, *11* (6), 372.

(8) Marchioro, A.; Teuscher, J.; Friedrich, D.; Kunst, M.; Van De Krol, R.; Moehl, T.; Grätzel, M.; Moser, J.-E. Unravelling the mechanism of photoinduced charge transfer processes in lead iodide perovskite solar cells. *Nat. Photonics* **2014**, *8* (3), 250.

(9) Park, K. S.; Lee, K. S.; Baek, J.; Lee, L.; Son, B. H.; Koo Lee, Y. E.; Ahn, Y. H.; Park, W. I.; Kang, Y.; Sung, M. M. Observation of Charge Separation and Space-Charge Region in Single-Crystal P3HT/C60 Heterojunction Nanowires. *Angew. Chem.* **2016**, *128* (35), 10429−10433.

(10) Duncan, W. R.; Prezhdo, O. V. Temperature independence of the photoinduced electron injection in dye-sensitized TiO2 rationalized by ab initio time-domain density functional theory. *J. Am. Chem. Soc.* **2008**, *130* (30), 9756−9762.

(11) Long, R.; Casanova, D.; Fang, W.-H.; Prezhdo, O. V. Donor−acceptor interaction determines the mechanism of photoinduced electron injection from graphene quantum dots into TiO2: π-stacking supersedes covalent bonding. *J. Am. Chem. Soc.* **2017**, *139* (7), 2619−2629.

(12) Souto, M.; Calbo, J.; Mañas-Valero, S.; Walsh, A.; Espallargas, G. M. Charge-transfer interactions between fullerenes and a mesoporous tetrathiafulvalene-based metal−organic framework. *Beilstein J. Nanotechnol.* **2019**, *10* (1), 1883−1893.

(13) Zhu, H.; Song, N.; Lian, T. Wave function engineering for ultrafast charge separation and slow charge recombination in type II core/shell quantum dots. *J. Am. Chem. Soc.* **2011**, *133* (22), 8762−8771.

(14) Xu, B.; Bi, D.; Hua, Y.; Liu, P.; Cheng, M.; Grätzel, M.; Kloo, L.; Hagfeldt, A.; Sun, L. A low-cost spiro [fluorene-9, 9′-xanthene]-based hole transport material for highly efficient solid-state dye-sensitized solar cells and perovskite solar cells. *Energy Environ. Sci.* **2016**, *9* (3), 873−877.

(15) Cao, Y.; Saygili, Y.; Ummadisingu, A.; Teuscher, J.; Luo, J.; Pellet, N.; Giordano, F.; Zakeeruddin, S. M.; Moser, J.-E.; Freitag, M. 11% efficiency solid-state dye-sensitized solar cells with copper (II/I) hole transport materials. *Nat. Commun.* **2017**, *8*, 15390.

(16) Ren, Y.; Sun, D.; Cao, Y.; Tsao, H. N.; Yuan, Y.; Zakeeruddin, S. M.; Wang, P.; Grätzel, M. A stable blue photosensitizer for color palette of dye-sensitized solar cells reaching 12.6% efficiency. *J. Am. Chem. Soc.* **2018**, *140* (7), 2405−2408.

(17) Mondal, S.; Yucknovsky, A.; Akulov, K.; Ghorai, N.; Schwartz, T.; Ghosh, H. N.; Amdursky, N. Efficient Photosensitizing Capabilities and Ultrafast Carrier Dynamics of Doped Carbon Dots. *J. Am. Chem. Soc.* **2019**, *141* (38), 15413−15422.

(18) Morteza Najarian, A.; Bayat, A.; McCreery, R. L. Orbital Control of Photocurrents in Large Area All-Carbon Molecular Junctions. *J. Am. Chem. Soc.* **2018**, *140* (5), 1900−1909.

(19) Brennan, L. J.; Byrne, M. T.; Bari, M.; Gun'ko, Y. K. Carbon nanomaterials for dye-sensitized solar cell applications: a bright future. *Adv. Energy Mater.* **2011**, *1* (4), 472−485.

(20) Kumar, U.; Sikarwar, S.; Sonker, R. K.; Yadav, B. Carbon nanotube: synthesis and application in solar cell. *J. Inorg. Organomet. Polym. Mater.* **2016**, *26* (6), 1231−1242.

(21) Liu, C.; Fan, Y.; Liu, M.; Cong, H.; Cheng, H.; Dresselhaus, M. S. Hydrogen storage in single-walled carbon nanotubes at room temperature. *Science* **1999**, *286* (5442), 1127−1129.

(22) Lee, S. M.; An, K. H.; Lee, Y. H.; Seifert, G.; Frauenheim, T. A hydrogen storage mechanism in single-walled carbon nanotubes. *J. Am. Chem. Soc.* **2001**, *123* (21), 5059−5063.

(23) Bonard, J. M.; Weiss, N.; Kind, H.; Stöckli, T.; Forró, L. s.; Kern, K.; Chatelain, A. Tuning the field emission properties of patterned carbon nanotube films. *Adv. Mater.* **2001**, *13* (3), 184−188.

(24) Hiraoka, T.; Yamada, T.; Hata, K.; Futaba, D. N.; Kurachi, H.; Uemura, S.; Yumura, M.; Iijima, S. Synthesis of single-and double-walled carbon nanotube forests on conducting metal foils. *J. Am. Chem. Soc.* **2006**, *128* (41), 13338−13339.

(25) Schroeder, V.; Savagatrup, S.; He, M.; Lin, S.; Swager, T. M. Carbon Nanotube Chemical Sensors. *Chem. Rev.* **2019**, *119* (1), 599−663.

(26) Weizmann, Y.; Chenoweth, D. M.; Swager, T. M. DNA− cnt nanowire networks for DNA detection. *J. Am. Chem. Soc.* **2011**, *133* (10), 3238−3241.

(27) Cao, Y.; Cong, S.; Cao, X.; Wu, F.; Liu, Q.; Amer, M. R.; Zhou, C. Review of electronics based on single-walled carbon nanotubes. *Single-Walled Carbon Nanotubes*; Springer: New York, 2019; pp 189−224.

(28) Zhang, L.; Zaric, S.; Tu, X.; Wang, X.; Zhao, W.; Dai, H. Assessment of chemically separated carbon nanotubes for nano-electronics. *J. Am. Chem. Soc.* **2008**, *130* (8), 2686−2691.

(29) Yu, L.; Shearer, C.; Shapter, J. Recent Development of Carbon Nanotube Transparent Conductive Films. *Chem. Rev.* **2016**, *116* (22), 13413−13453.

(30) Jeon, I.; Matsuo, Y.; Maruyama, S. Single-walled carbon nanotubes in solar cells. *Single-Walled Carbon Nanotubes*; Springer: New York, 2019; pp 271−298.

(31) Sarkar, R.; Habib, M.; Pal, S.; Prezhdo, O. V. Ultrafast, asymmetric charge transfer and slow charge recombination in porphyrin/CNT composites demonstrated by time-domain atomistic simulation. *Nanoscale* **2018**, *10* (26), 12683−12694.

(32) Sarkar, R.; Habib, M.; Pal, S.; Prezhdo, O. V. Tuning charge transfer and recombination in exTTF/CNT nanohybrids by choice of chalcogen: A time-domain density functional analysis. *J. Appl. Phys.* **2021**, *129* (2), 025501.

(33) Yan, J.; Uddin, M.; Dickens, T.; Okoli, O. Carbon nanotubes (CNTs) enrich the solar cells. *Sol. Energy* **2013**, *96*, 239−252.

(34) Pal, S.; Casanova, D.; Prezhdo, O. V. Effect of aspect ratio on multiparticle auger recombination in single-walled carbon nanotubes: time domain atomistic simulation. *Nano Lett.* **2018**, *18* (1), 58−63.

(35) Chaban, V. V.; Pal, S.; Prezhdo, O. V. Laser-induced explosion of nitrated carbon nanotubes: nonadiabatic and reactive molecular

https://doi.org/10.1021/jacs.1c02325
J. Am. Chem. Soc. 2021, 143, 6649−6656

dynamics simulations. *J. Am. Chem. Soc.* **2016**, *138* (49), 15927−15934.
(36) Avlasevich, Y.; Li, C.; Müllen, K. Synthesis and applications of core-enlarged perylene dyes. *J. Mater. Chem.* **2010**, *20* (19), 3814−3826.
(37) Herrmann, A.; Müllen, K. From industrial colorants to single photon sources and biolabels: The fascination and function of rylene dyes. *Chem. Lett.* **2006**, *35* (9), 978−985.
(38) Li, C.; Wonneberger, H. Perylene imides for organic photovoltaics: yesterday, today, and tomorrow. *Adv. Mater.* **2012**, *24* (5), 613−636.
(39) Liu, Z.; Wu, Y.; Zhang, Q.; Gao, X. Non-fullerene small molecule acceptors based on perylene diimides. *J. Mater. Chem. A* **2016**, *4* (45), 17604−17622.
(40) Lee, J.-H.; Yoon, S.-M.; Kim, K. K.; Cha, I.-S.; Park, Y. J.; Choi, J.-Y.; Lee, Y. H.; Paik, U. Exfoliation of Single-Walled Carbon Nanotubes Induced by the Structural Effect of Perylene Derivatives and Their Optoelectronic Properties. *J. Phys. Chem. C* **2008**, *112* (39), 15267−15273.
(41) Tsarfati, Y.; Strauss, V.; Kuhri, S.; Krieg, E.; Weissman, H.; Shimoni, E.; Baram, J.; Guldi, D. M.; Rybtchinski, B. Dispersing Perylene Diimide/SWCNT Hybrids: Structural Insights at the Molecular Level and Fabricating Advanced Materials. *J. Am. Chem. Soc.* **2015**, *137* (23), 7429−7440.
(42) Backes, C.; Hauke, F.; Hirsch, A. The potential of perylene bisimide derivatives for the solubilization of carbon nanotubes and graphene. *Adv. Mater.* **2011**, *23* (22−23), 2588−2601.
(43) Dirian, K.; Herranz, M. A.; Katsukis, G.; Malig, J.; Rodríguez-Pérez, L.; Romero-Nieto, C.; Strauss, V.; Martín, N.; Guldi, D. M. Low dimensional nanocarbons−chemistry and energy/electron transfer reactions. *Chem. Sci.* **2013**, *4* (12), 4335−4353.
(44) Chitta, R.; D'Souza, F. Self-assembled tetrapyrrole−fullerene and tetrapyrrole−carbon nanotube donor−acceptor hybrids for light induced electron transfer applications. *J. Mater. Chem.* **2008**, *18* (13), 1440−1471.
(45) D'Souza, F.; Sandanayaka, A. S.; Ito, O. SWNT-based supramolecular nanoarchitectures with photosensitizing donor and acceptor molecules. *J. Phys. Chem. Lett.* **2010**, *1* (17), 2586−2593.
(46) Hasobe, T. Supramolecular nanoarchitectures for light energy conversion. *Phys. Chem. Chem. Phys.* **2010**, *12* (1), 44−57.
(47) Sgobba, V.; Rahman, G. A.; Guldi, D. M.; Jux, N.; Campidelli, S.; Prato, M. Supramolecular assemblies of different carbon nanotubes for photoconversion processes. *Adv. Mater.* **2006**, *18* (17), 2264−2269.
(48) Guldi, D. M.; Taieb, H.; Rahman, G. A.; Tagmatarchis, N.; Prato, M. Novel photoactive single-walled carbon nanotube−porphyrin polymer wraps: efficient and long-lived intracomplex charge separation. *Adv. Mater.* **2005**, *17* (7), 871−875.
(49) Kang, H. S.; Sisto, T. J.; Peurifoy, S.; Arias, D. H.; Zhang, B.; Nuckolls, C.; Blackburn, J. L. Long-lived charge separation at heterojunctions between semiconducting single-walled carbon nanotubes and perylene diimide electron acceptors. *J. Phys. Chem. C* **2018**, *122* (25), 14150−14161.
(50) Oelsner, C.; Schmidt, C.; Hauke, F.; Prato, M.; Hirsch, A.; Guldi, D. M. Interfacing strong electron acceptors with single wall carbon nanotubes. *J. Am. Chem. Soc.* **2011**, *133* (12), 4580−4586.
(51) Ehli, C.; Oelsner, C.; Guldi, D. M.; Mateo-Alonso, A.; Prato, M.; Schmidt, C.; Backes, C.; Hauke, F.; Hirsch, A. Manipulating single-wall carbon nanotubes by chemical doping and charge transfer with perylene dyes. *Nat. Chem.* **2009**, *1* (3), 243−249.
(52) Hedström, S.; Chaudhuri, S.; La Porte, N. T.; Rudshteyn, B.; Martinez, J. F.; Wasielewski, M. R.; Batista, V. S. Thousandfold enhancement of photoreduction lifetime in Re (bpy)(CO) 3 via spin-dependent Electron transfer from a perylenediimide radical anion donor. *J. Am. Chem. Soc.* **2017**, *139* (46), 16466−16469.
(53) Sharma, P. P.; Wu, J.; Yadav, R. M.; Liu, M.; Wright, C. J.; Tiwary, C. S.; Yakobson, B. I.; Lou, J.; Ajayan, P. M.; Zhou, X. D. Nitrogen-doped carbon nanotube arrays for high-efficiency electrochemical reduction of CO2: on the understanding of defects, defect density, and selectivity. *Angew. Chem., Int. Ed.* **2015**, *54* (46), 13701−13705.
(54) Mleczko, L.; Lolli, G. Carbon nanotubes: an example of multiscale development—a mechanistic view from the subnanometer to the meter scale. *Angew. Chem., Int. Ed.* **2013**, *52* (36), 9372−9387.
(55) Habenicht, B. F.; Prezhdo, O. V. Nonradiative quenching of fluorescence in a semiconducting carbon nanotube: A time-domain ab initio study. *Phys. Rev. Lett.* **2008**, *100* (19), 197402.
(56) Habenicht, B. F.; Kamisaka, H.; Yamashita, K.; Prezhdo, O. V. Ab initio study of vibrational dephasing of electronic excitations in semiconducting carbon nanotubes. *Nano Lett.* **2007**, *7* (11), 3260−3265.
(57) Pal, S.; Trivedi, D. J.; Akimov, A. V.; Aradi, B.; Frauenheim, T.; Prezhdo, O. V. Nonadiabatic Molecular Dynamics for Thousand Atom Systems: A Tight-Binding Approach toward PYXAID. *J. Chem. Theory Comput.* **2016**, *12* (4), 1436−1448.
(58) Akimov, A. V.; Prezhdo, O. V. The PYXAID program for non-adiabatic molecular dynamics in condensed matter systems. *J. Chem. Theory Comput.* **2013**, *9* (11), 4959−4972.
(59) Akimov, A. V.; Prezhdo, O. V. Advanced capabilities of the PYXAID program: integration schemes, decoherence effects, multi-excitonic states, and field-matter interaction. *J. Chem. Theory Comput.* **2014**, *10* (2), 789−804.
(60) Vinten, P.; Marshall, P.; Lefebvre, J.; Finnie, P. Thermodynamic and energetic effects on the diameter and defect density in single-walled carbon nanotube synthesis. *J. Phys. Chem. C* **2013**, *117* (7), 3527−3536.
(61) Yuan, Q.; Xu, Z.; Yakobson, B. I.; Ding, F. Efficient defect healing in catalytic carbon nanotube growth. *Phys. Rev. Lett.* **2012**, *108* (24), 245505.
(62) Mann, C.; Hertel, T. 13 nm Exciton Size in (6, 5) Single-Wall Carbon Nanotubes. *J. Phys. Chem. Lett.* **2016**, *7* (12), 2276−2280.
(63) Wang, F.; Dukovic, G.; Brus, L. E.; Heinz, T. F. The optical resonances in carbon nanotubes arise from excitons. *Science* **2005**, *308* (5723), 838−841.
(64) Mandal, B.; Sarkar, S.; Sarkar, P. Energetics and electronic structure of encapsulated graphene nanoribbons in carbon nanotube. *J. Phys. Chem. A* **2013**, *117* (36), 8568−8575.
(65) Malola, S.; Häkkinen, H.; Koskinen, P. Raman spectra of single-walled carbon nanotubes with vacancies. *Phys. Rev. B: Condens. Matter Mater. Phys.* **2008**, *77* (15), 155412.
(66) Brown, K. E.; Veldkamp, B. S.; Co, D. T.; Wasielewski, M. R. Vibrational dynamics of a perylene−perylenediimide donor−acceptor dyad probed with femtosecond stimulated Raman spectroscopy. *J. Phys. Chem. Lett.* **2012**, *3* (17), 2362−2366.
(67) Angelella, M.; Wang, C.; Tauber, M. J. Resonance Raman spectra of a perylene bis (dicarboximide) chromophore in ground and lowest triplet states. *J. Phys. Chem. A* **2013**, *117* (38), 9196−9204.
(68) Habenicht, B. F.; Craig, C. F.; Prezhdo, O. V. Time-domain ab initio simulation of electron and hole relaxation dynamics in a single-wall semiconducting carbon nanotube. *Phys. Rev. Lett.* **2006**, *96* (18), 187401.
(69) Son, M.; Park, K. H.; Yoon, M.-C.; Kim, P.; Kim, D. Excited-state vibrational coherence in perylene bisimide probed by femtosecond broadband pump−probe spectroscopy. *J. Phys. Chem. A* **2015**, *119* (24), 6275−6282.
(70) Mukamel, S. *Principles of Nonlinear Optical Spectroscopy*; Oxford University Press on Demand: New York, 1999.
(71) Kilina, S. V.; Neukirch, A. J.; Habenicht, B. F.; Kilin, D. S.; Prezhdo, O. V. Quantum zeno effect rationalizes the phonon bottleneck in semiconductor quantum dots. *Phys. Rev. Lett.* **2013**, *110* (18), 180404.
(72) Münich, P. W.; Schierl, C.; Dirian, K.; Volland, M.; Bauroth, S.; Wibmer, L.; Syrgiannis, Z.; Clark, T.; Prato, M.; Guldi, D. M. Tuning the Carbon Nanotube Selectivity: Optimizing Reduction Potentials and Distortion Angles in Perylenediimides. *J. Am. Chem. Soc.* **2018**, *140* (16), 5427−5433.
(73) Englman, R.; Jortner, J. The energy gap law for radiationless transitions in large molecules. *Mol. Phys.* **1970**, *18* (2), 145−164.

https://doi.org/10.1021/jacs.1c02325
J. Am. Chem. Soc. 2021, 143, 6649−6656